

Highly Adaptive Triboelectric-Electromagnetic Hybrid Nanogenerator for Scavenging Flow Energy and Self-Powered Marine Wireless Sensing

Yawei Wang, Zian Qian, Cong Zhao, Yan Wang, Kun Jiang, Junpeng Wang, Zhaochen Meng, Fangming Li, Chuanqing Zhu, Pengfei Chen, Hao Wang,* and Minyi Xu*

With the development of the smart ocean which contains a large number of wireless sensor nodes, it is a great demand to develop high-performance marine energy harvesters for powering those sensors. In this work, a highly adaptive hybrid nanogenerator based on triboelectric nanogenerator and electromagnetic generator is proposed. The hybrid nanogenerator can be used for scavenging both wind energy and ocean current energy. The peak power of the hybrid nanogenerator can reach 449.74 mW, which can recharge a 50 mAh-3.7 V Lithium battery. In addition, it is found that there is a linear relationship between the voltage frequency of the triboelectric nanogenerator and the rotation speed, indicating the hybrid nanogenerator can serve as a flow velocity sensor. A fully self-powered marine wireless sensor node is fabricated based on the hybrid nanogenerator and management circuit. The demonstrations show that the present hybrid nanogenerator has great potential applications for marine wireless sensing in the scenarios of nearshore, offshore, and underwater.

1. Introduction

The development of the smart ocean requires a large number of distributed marine wireless sensor nodes.^[1–4] Those marine wireless sensor nodes are mainly powered by batteries. But the lifespan of the batteries limits the development of the smart ocean and makes a threat to the environment. Self-powered sensor nodes are capable to supply power by harvesting energy

from the surrounding environment,^[5] which could be a promising approach to solving this problem. Blue energy is abundantly distributed in the marine environment, such as marine current energy, wave energy, and ocean wind energy.^[6] It has a wide range, high energy density, and stable output. Effective energy conversion technology can meet the needs of distributed sensors.


Nowadays, the capture of blue energy has become a research hotspot.^[7–13] Piezoelectric generators (PENG),^[14,15] electromagnetic generators (EMG),^[16] and triboelectric nanogenerator (TENG)^[17–19] are widely used in harvesting blue energy. Among them, TENG stands out because of its simple design, low cost, and high robustness.^[20–23] Various methods are proposed to enhance the output of the TENG, such as structure optimization,

^[24–27] charge excitation,^[28] charge pumping,^[29] and power management.^[30] However, the TENGs are still limited by their low current and high internal resistance, which hinders further application as energy harvesters to power the electronics such as MCU and Wi-Fi module in wireless sensor nodes.

Hybridizing the triboelectric with other techniques, such as electromagnetic,^[31,32] piezoelectric,^[33] and photovoltaic,^[34] has become a possible way to improve the energy harvesting efficiency of the whole system. Among them, the combination of TENG and EMG has become the most desirable method to raise energy scavenging efficiency.^[30,35–38] Zhong et al. first proposed a hybrid electromagnetic-triboelectric nanogenerator to harvest energy in 2015.^[39] By integrating these two energy conversion technologies, the hybrid nanogenerator has an ultra-high output performance^[38,40–42] and broadens the frequency range of energy harvesting.^[35,37,43] This allows nanogenerators to have a greater range of applications, such as charging super capacitors,^[43] powering commercial sensors,^[35,42] self-powered sensing,^[44–46] etc. However, most previous works need an external power supply for processing the signal, and the trigger to supply power to the sensor from the hybrid generator is manual rather than automatic. This makes it hard to realize practical applications in a distributed environment.

Y. Wang, Z. Qian, C. Zhao, Y. Wang, K. Jiang, J. Wang, Z. Meng, F. Li, C. Zhu, H. Wang, M. Xu
Dalian Key Lab of Marine Micro/Nano Energy and Self-powered Systems
Marine Engineering College
Dalian Maritime University
Dalian 116026, China
E-mail: hao8901@dlmu.edu.cn; xuminyi@dlmu.edu.cn

P. Chen
Beijing Institute of Nanoenergy and Nanosystems
Chinese Academy of Sciences
Beijing 100085, China

 The ORCID identification number(s) for the author(s) of this article can be found under <https://doi.org/10.1002/admt.202201245>.

DOI: 10.1002/admt.202201245

In this work, a triboelectric-electromagnetic hybrid nanogenerator (TEHN) is proposed to scavenge wind energy and marine current energy to realize fully self-powered marine wireless sensor nodes. The electrical performance of the TEHN was systematically analyzed. The peak power of the present TEHN reaches 449.74 mW, which can recharge a 50 mAh-3.7 V Lithium battery. Besides, the TEHN can serve as a self-powered sensor to detect flow velocity and process data locally by a signal processing module. Moreover, the self-powered marine wireless sensing is achieved by TEHN successfully, and it can automatically complete the periodic wireless signal transmission by an external timer. Finally, the demonstrations show that the TEHN is able to work nearshore, offshore, and underwater. The high performance and high adaptability exhibit the potential in the application of the marine environment.

2. Results and Discussion

2.1. Structures and Working Principle of the TEHN

Figure 1a exhibits the blueprint of this work, the TEHN can be applied in several marine scenarios including harvesting nearshore, offshore wind energy and underwater current energy. Through the hybrid nanogenerator and the rotary structure, the TEHN served as a self-powered sensor as well as a marine flow energy harvester, which provides a reliable solution to self-powered wireless sensor nodes. Figure 1b exhibits the 3D explosion diagram of the TEHN, which is composed of three parts: turbine, shaft, and hybrid nanogenerator (EMG and TENG). By selecting the vertical axis mode turbine, TEHN can conveniently be placed in the marine environment to harvest

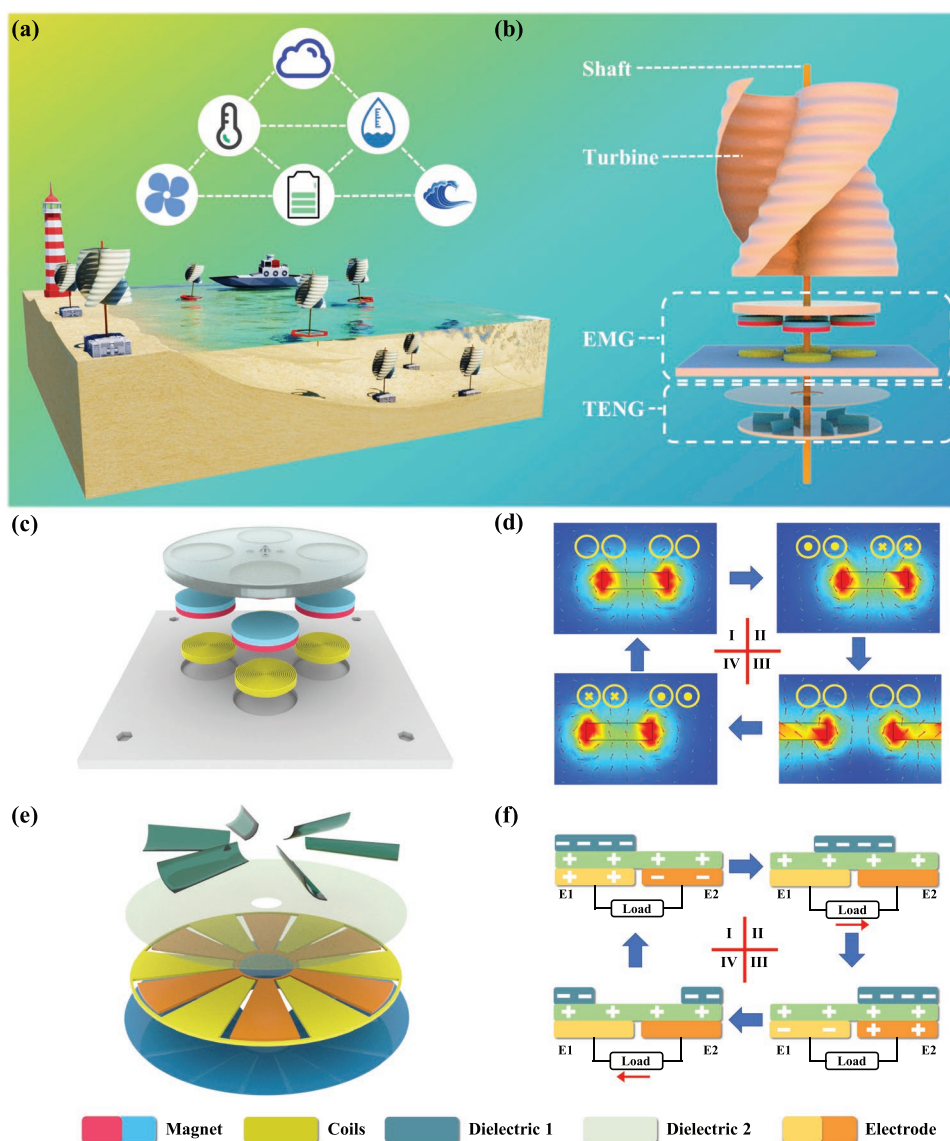


Figure 1. The design and working principle of the TEHN. a) Sense graph of the TEHN in marine environment. b) 3D explosion diagram of the TEHN. Schematic diagram and the working principle of the EMG (c,d) and TENG (e,f).

low-grade energy. The turbine rotates under the excitation of fluid (such as wind and water). Then the hybrid nanogenerator rotates along with the motion of the turbine through the shaft. Finally, the marine flow energy is converted to electrical energy through EMG and TENG.

Figure 1c exhibits the detailed structure of the EMG, which involved a rotor and a stator. Four magnets with the same magnetic pole are inserted into the rotor. The stator is composed of four coils (50 mm in diameter) arranged homogeneously apart. The working principle of the EMG is based on electromagnetic induction (Figure 1d). In State I, the magnet is in alignment with the coils, and the magnetic flux through the coil is at the maximum value. As the rotor spins, the magnetic flux in the coils decreases, creating an induced current (State II) due to Lenz's Law. The current keeps the direction until the magnetic flux in the coil reaches its minimum value (Stage III). In Stage IV, the magnetic flux in the coil increases as the magnets move continuously, creating a back-induced current. The open-circuit voltage (V_{oc}^{EMG}) and short-circuit current (I_{sc}^{EMG}) of the EMG can be presented as:

$$V_{oc}^{EMG} = \frac{d\Phi}{dt} = N \frac{SdB}{dt} \quad (1)$$

$$I_{sc}^{EMG} = \frac{V_{oc}^{EMG}}{R} \quad (2)$$

where Φ is the magnetic flux, t is the time, N is the number of coil turns, S is the area of the coil, B is the magnetic flux density, and R is the resistance of the coil. Considering the Equation (1) and (2), with the increasing number of coils turns and magnetic flux, V_{oc}^{EMG} and the I_{sc}^{EMG} both increase proportionally.

As depicted in Figure 1e, the TENG is also composed of a rotor and a stator. Six PVC films function as the rotor and the dielectric layer. The stator is composed of a PCB board and a dielectric layer. Six pairs of Cu are deposited on the PCB board as electrodes. A nylon film is covered on the electrodes as the dielectric layer. The working process of the TENG mainly contains two steps: an initial contact charging and a cyclic rotating electrostatic induction. As for the contact charging, due to the difference in electronegativity, PVC and Nylon are charged with an equal number of charges with opposite polarities. The charge accumulation process can be seen in Figure S1 (Supporting Information). The transfer charge increases from 17 to 120 nC and keeps stable, which means the charge transfer due to the contact charging reaches saturation. As for the electrostatic induction, assuming that the contact area of the PVC is half of Nylon, according to the law of conservation of charge, the negative charge density of PVC is twice the positive charge density of Nylon. Figure 1f illustrates the electrostatic induction procession, and it consists of four stages in one spin cycle. In stage I, the PVC film is aligned to the E1. Due to the charges on the PVC and Nylon, E1 and E2 are induced the positive and negative charges. As the rotor spins, the electrons will flow from E2 to E1, creating a current in the right direction until Stage III. In Stage IV, as the PVC film continues to move, electrons will be transferred from E1 to E2, creating a leftward current in the circuit until another PVC film fully moves to the top of E1 equivalent to the initial state.

2.2. Electrical Performance

A servo motor is served as an external excitation to study the output performance of the TEHN. The rotating speed of TENG can be adjusted precisely through the control module. The effect of the number of magnets on electric performance is shown in Figure 2a,b. Under the 300 rpm rotation speed, the V_{oc}^{EMG} and I_{sc}^{EMG} increase from 0.39 V, 2.07 mA to 1.39 V, 8.19 mA as the number of magnets varies from 1 to 4. Besides, the output of the EMG is related to the distance between the magnet and coil(D1). The V_{oc}^{EMG} increases from 0.18 V to 10.93V with the D1 reducing from 5 to 0.4 cm under 300 rpm rotating speed (Figure 2c). The main reason is that the reduction of the distance increases the magnetic flux density in the coil. Four magnets and a 0.5 cm distance of D1 are chosen to make EMG a better output performance, as well as a smooth operation. The relationship between the choice of dielectric material and the output performance of the TENG is investigated. PTFE or PVC is chosen as electronegative material, while Nylon is chosen as electropositive material. Cu is selected as the electrode material. The performance of the TENG under various material combinations was tested in two modes (dielectric-dielectric mode and dielectric-conductor mode). The working principle of the dielectric-conductor mode is shown in Figure S2 (Supporting Information). Figure 2d,e shows that the PVC-Nylon-Cu yields the best output performance in V_{oc}^{TENG} and I_{sc}^{TENG} . Therefore, the material combination of PVC-Nylon-Cu was chosen for the further testing. The relationship between the distance of the PVC and Nylon layer (D2) and the output performance is studied in Figure 2f. With D2 dropping from 3.5 to 0.5 cm, the short-circuit transferred charge (Q_{sc}^{TENG}) increases from 29.21 nC to 270.46 nC. The main reason is that the reduction of D2 increases the effective contact between Nylon and PVC. However, Q_{sc}^{TENG} of the TENG starts to decrease as the distance is less than 0.5 cm. It is likely that the narrow distance causes the PVC to bend and decrease the effective contact area. The Q_{sc}^{TENG} , V_{oc}^{TENG} and I_{sc}^{TENG} can be determined in the following equations.^[47,48]

$$Q_{sc}^{TENG} = \int_0^l \frac{\sigma\omega dk}{1 + \left[\frac{c_2(k)}{c_1(k)} \right]_{x=g+l}} - \int_0^l \frac{\sigma\omega dk}{1 + \left[\frac{c_2(k)}{c_1(k)} \right]_{x=0}} \quad (3)$$

$$V_{oc}^{TENG} = \frac{Q_{sc}^{TENG}}{C} \quad (4)$$

$$I_{sc}^{TENG} = \frac{d(Q_{sc}^{TENG})}{dt} \quad (5)$$

σ is the tribo-charges density, ω is the width of the PVC. Assuming that dk is a small region in the bottom of the PVC containing tribo-charges. The total charges on E1 and E2 are $\sigma\omega dk$. $C_i(k)$ is the capacitance between the small region and the metal electrode. Referring to Equations (4) and (5), with the increase of the Q_{sc}^{TENG} , both V_{oc}^{TENG} and I_{sc}^{TENG} increase proportionally. Therefore, D2 of 0.5 cm is chosen to achieve the best electrical performance of TENG.

The relationship between the rotation frequency and the output of the generator (EMG and TENG) is studied. With

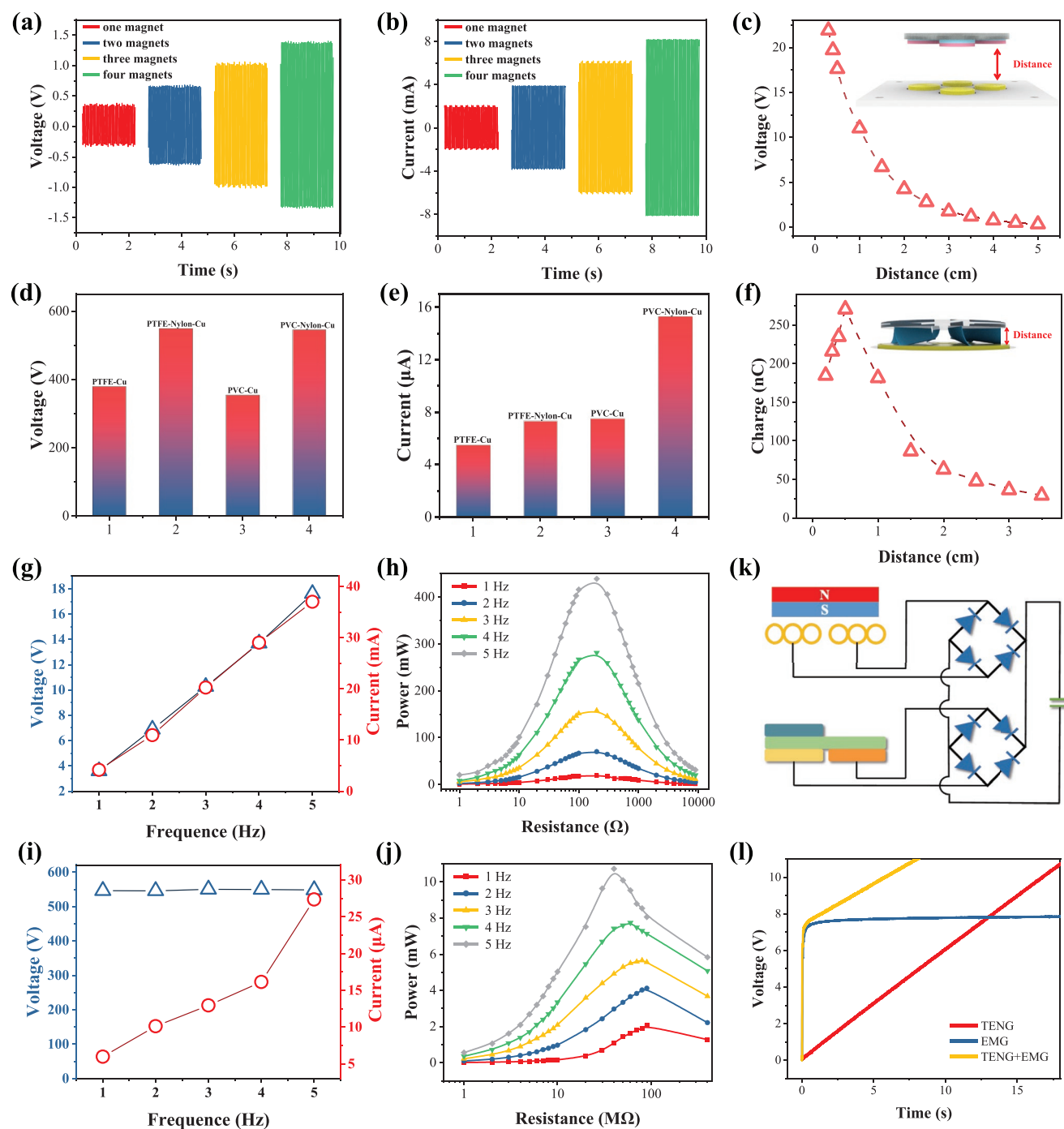


Figure 2. Electrical outperformance of the TEHN. The relationship of a) V_{oc}^{EMG} and b) I_{sc}^{EMG} of changing magnet number. c) The V_{oc}^{EMG} of changing the distance between magnets and coils. d) V_{oc}^{TENG} and e) I_{sc}^{TENG} with various materials. f) V_{oc}^{TENG} of changing the distance between stator and rotor. g) V_{oc}^{EMG} , I_{sc}^{EMG} and peak power of EMG h) in different rotation frequencies. i) V_{oc}^{TENG} , I_{sc}^{TENG} and peak power of TENG j) in different rotation frequencies. k) Schematic drawing of the hybridized generator connected parallelly to charge a capacitor. l) The comparison of the charging performance for a capacitor (10 μ F).

the rotation, the frequency varies from 1 Hz to 5 Hz, the V_{oc}^{EMG} and the I_{sc}^{EMG} increase from 3.59 V, 4.16 mA to 17.61 V, 37 mA (Figure 2g). The corresponding maximum peak power of the EMG is 18.96, 70.06, 157.98, 281.26, and 439.01mW with various rotation frequencies when the external resistance is 200 Ω (Figure 2h). As depicted in Figure 2i, the V_{oc}^{TENG} almost keeps

stable at 550V in the same condition, while I_{sc}^{TENG} increases from 5.99 μ A to 27.35 μ A. Figure 2j shows the relationship between the peak power of the TENG and the external resistance. The maximum peak power is 2.05, 4.12, 5.58, 7.75, and 10.73 mW, corresponding to the external resistance of 90, 90, 80, 60, and 40 M Ω , respectively (as the rotation frequency increases

from 1 Hz to 5 Hz). Then, the TENG and EMG are connected to a rectifier parallel to charge a 10 μ F capacitor (as indicated in Figure 2k). The charging voltage can be significantly improved when the TENG and EMG work simultaneously, as shown in Figure 2l.

The flow velocity (wind flow velocity and water flow velocity) is a vital parameter in the marine environment. Compare to traditional flow velocity sensors, the advantages of self-powered and robustness make TENG a potential sensing technology in the future. **Figure 3a** displays the original voltage signal of the TENG under the rotating speed of 300 rpm. Due to the feature of the TENG structure, the frequency of the signal is more than six times the rotation frequency of the TENG. The signal after Fast Fourier Transform processing is shown in **Figure 3b**. The result reveals that the peak value occurs at 29.985 Hz (the error is negligible compared to the theoretical value of 30 Hz). With the various rotation speeds, the voltage frequency also changes as indicated in **Figure 3c**, which proves the capability of the TENG as a self-powered sensor. As indicated in **Figure 3d,e**, both correlation coefficients between the frequency and wind flow, and water flow velocity prove to be 0.98, which exhibits

a good linear relationship between them. The electrical circuit of the signal processing module is illustrated in **Figure 3f(i)**, which consists of two filter capacitors, an amplitude module, and an MCU. The photograph of the signal processing module is shown in **Figure S3** (Supporting Information). With the help of the amplification module, the sinusoidal waveform V1 is converted into a square waveform V2 (**Figure 3f(ii)**), and then transmitted to the MCU for further processing. Subsequently, we compare the working performance of the TEHN with the commercial flow velocity sensors through a wind turbine (**Figure 3g**) and a circulating water tunnel (**Figure 3h**), proving that the TEHN has a reliable sensing capability. The corresponding demonstration can be seen in **Videos S1** and **S2** (Supporting Information), respectively.

2.3. Power Management Strategy for TEHN

A large number of distributed wireless sensor nodes is required to realize marine environment monitoring. The limited service time of traditional batteries poses great challenges to the

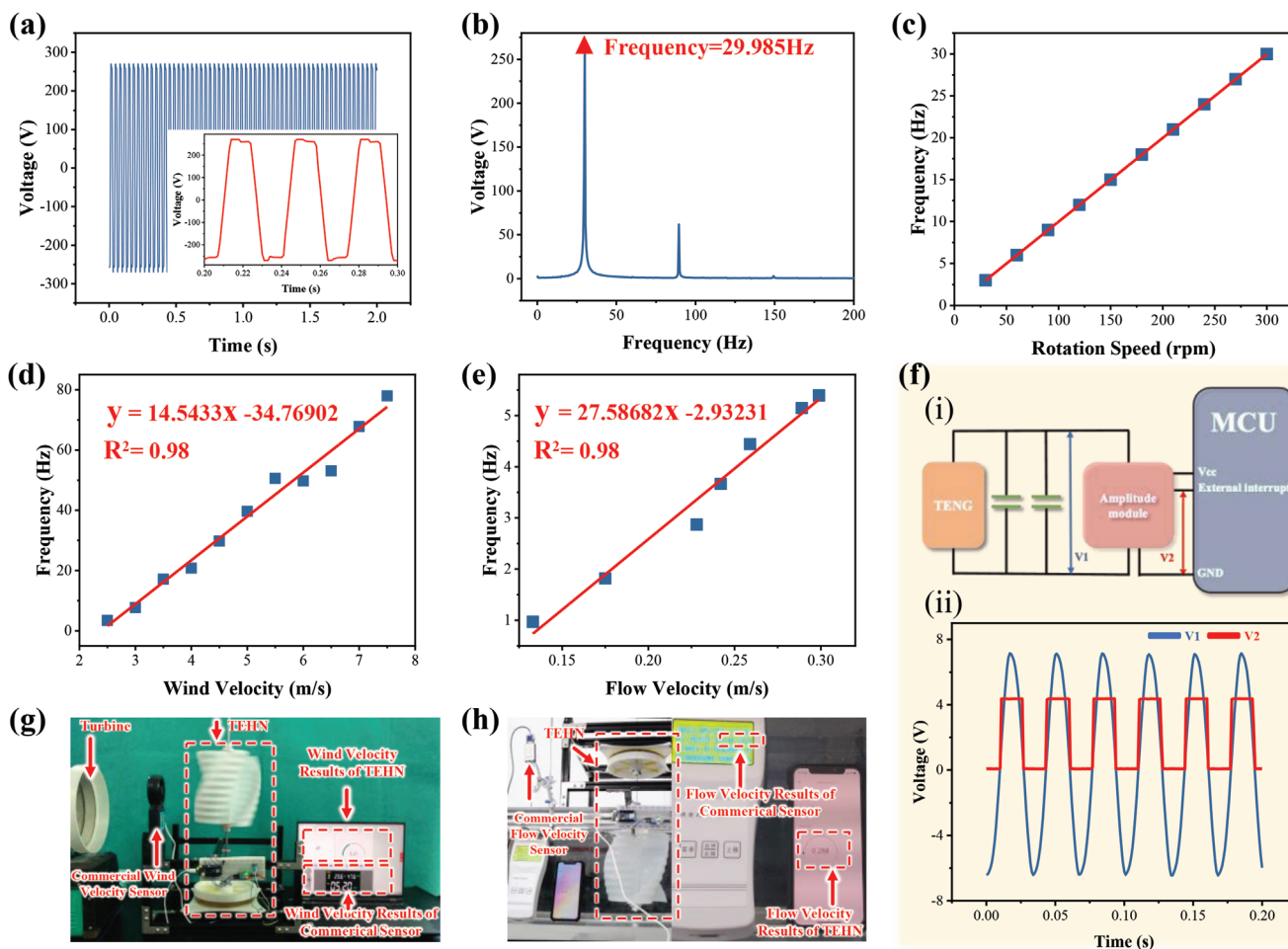


Figure 3. The flow velocity detection performance of the TEHN. a) The original signal of the TENG (the inset indicates the TENG signal within 0.1s) and the Fast Fourier Transform results (b). c) The relationship between the signal frequency rotation speed. The relationship of wind velocity (d) and water current velocity (e) with the electrical signal frequency. f) The illustration of the self-powered flow velocity sensor. i) The circuit of the self-powered flow velocity detection system. ii) Voltage signal of the TENG after transformation processing. Demonstration for detecting the wind velocity (g) and flow velocity (h) in real-time.

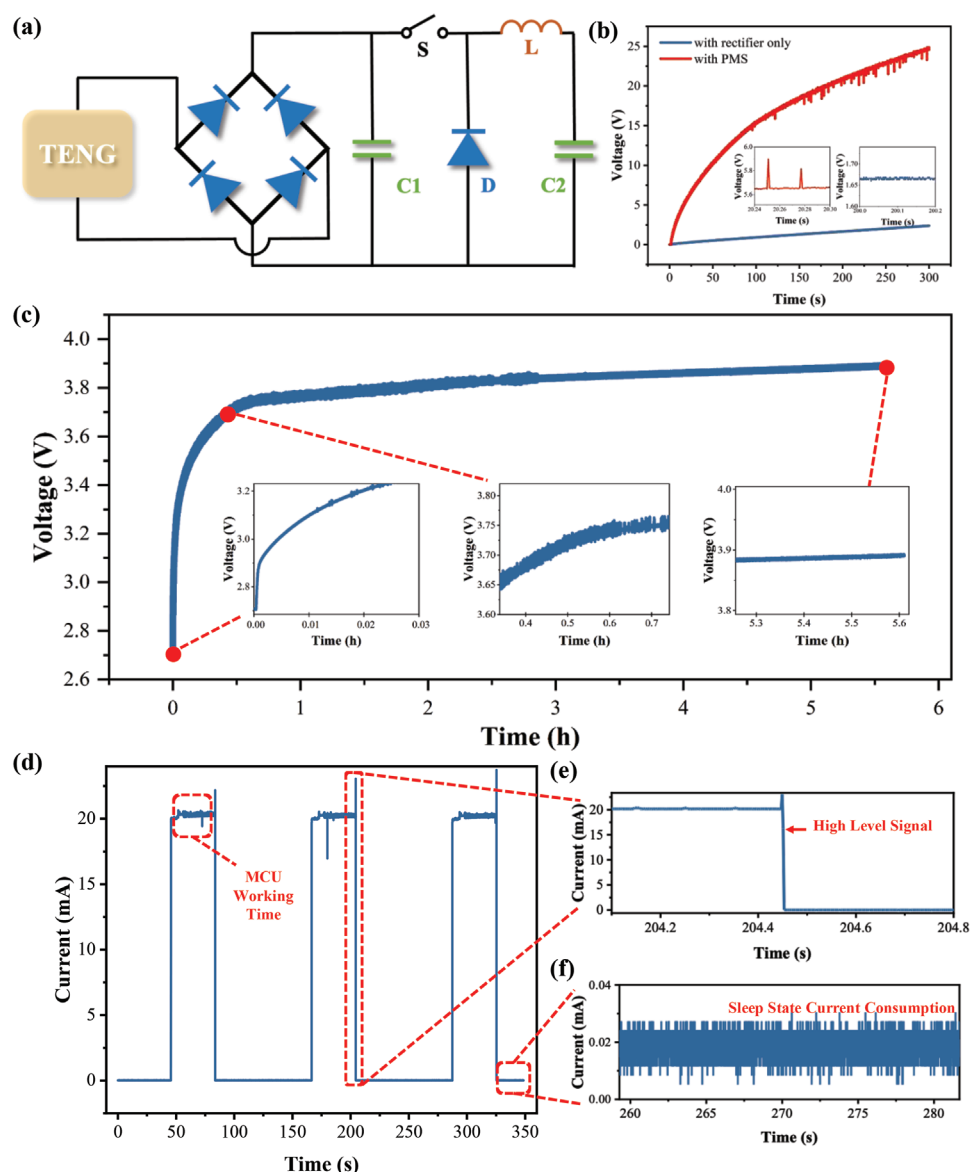


Figure 4. Realization of self-powered system. a) The circuit diagram of the power management system (PMS) for TENG. b) Charging curve with a single rectifier and PMS to charge 4700 μF capacitor. c) (50mAh-3.7V) Lithium battery charging performance with TEHN. d) The operating current of the self-driven system, and the high-level signal (e), and sleep state current consumption (f).

continuous operation of wireless sensor nodes. Although TENG owns a relatively high voltage output, the inner resistance restricts the performance in recharging. A power management system (PMS) is proposed to improve the charging efficiency of the TENG significantly. The circuit diagram of the PMS is depicted in Figure 4a. The PMS consists of a rectifier, a capacitor C1, a switch S, a diode D, and an inductor L. First, the switch is turned off, and the rectifier converts the AC output to DC to charge C1. Then, as the voltage of C1 reaches the threshold value, the switch S is closed and the energy of C1 is transferred to C2 and L until the voltage of C1 drops to zero. Finally, S is off, and the electrical energy temporarily stored in the L-C1 unit flows to C2 through the conducted D. As the PMS operates continuously, the energy stored in C2 can be improved. The TENG with only a single rectifier charges a 4700 μF capacitor to 2.4 V

within 300 s, while the TENG with the PMS charges it to 24.6 V (Figure 4b). The two insets illustrate the different charging curves with PMS and rectifier, which are characterized by pulse rise and smooth rise, respectively. As for the practical applications of the TEHN, we recharge a 50 mAh-3.7 V Lithium battery which could supply power to MCU steadily. The battery is charged from 2.7 V to 3.89 V by TEHN within 5.61h (Figure 4c). The three insets demonstrate the charging states at different steps from the initial step with a fast growth rate to the final step with a steady rate.

In order to realize self-powered monitoring for the marine environment without any external power supply, a reliable power management strategy is needed. This strategy should allow the TEHN power to the electrical equipment automatically, and be able to reduce power consumption. An

external timer is used to manage the power supply of the system periodically. Figure 4d presents the current consumption of the system under the control of the timer. The operating current of the MCU is $\approx 20\text{mA}$. When the operation is done, the MCU will send a high-level signal (Figure 4e) to the timer to cut off the power supply to MCU, then the current consumption will drop to $20\ \mu\text{A}$ (Figure 4f). As the sleep time is over, the timer will recover the power supply to MCU until the next high-level signal. The sleep time can be controlled by adjusting the timer's resistor, which allows the TEHN to have enough time to harvest energy to supplement the consumption of the MCU. Significantly, the MCU can be automatically triggered to work, enabling fully self-powered sensing in real environments.

2.4. Demonstration of the TEHN

Figure 5a indicates the process of harvesting energy and realizing self-powered environmental monitoring. Under the excitation of the fluid flow, the electricity generated by the TENG and EMG is managed by the PMS to charge the battery. Simultaneously, the TENG and other commercial sensors can acquire the information of wind flow velocity, water flow velocity, temperature, and humidity, and then transmit them to the MCU. On top of that, the TEHN can work in various marine scenarios (e.g., nearshore, offshore, and underwater). Figure 5b and Video S3 (Supporting Information) show that the TEHN can harvest the wind energy and transmit the sensing data to the IoT cloud periodically. The timer's sleep time is adjusted to 1 min in the demonstration. The TEHN can harvest wind energy near shore and store it in the battery. When the MCU is powered on, the TEHN and commercial sensors start to obtain real-time environmental information (wind velocity, temperature, and humidity), and the timer will cut off the power supply after the sensor information is uploaded to the IoT cloud. In

areas with stable wind energy, the TEHN can work stably and independently without an external power source.

Actually, buoys that are widely distributed on the ocean surface play a key role in navigation guidance. By integrating with a float, the TEHN can scavenge offshore wind energy. The TEHN integrated with a float can power five LED lights under the excitation of wind (Figure 5c) and Video S4, Supporting Information). This demonstration shows that the TEHN is capable of harvesting wind energy offshore, and its potential applications in navigation buoys. Moreover, the TEHN can also harvest underwater current energy after installing the water-proof case and dynamic sealing unit. As a demonstration, the TEHN could light 24 LEDs under the excitation of underwater current as illustrated in Figure 5d and Video S5 (Supporting Information), which shows the characteristics of the TEHN that can operate underwater to harvest marine current energy.

3. Conclusion

In summary, a triboelectric-electromagnetic hybrid nanogenerator has been proposed for scavenging flow energy and self-powered marine sensing. The electrical output performance of the EMG and the TENG is investigated. The maximum voltage of TENG can reach 550 V, the maximum current of EMG is 37 mA, and the peak power of TEHN can reach 449.74 mW. Besides, TEHN is able to serve as a self-powered sensor to detect the flow velocity. With the wind turbine and the recirculating water tunnels, the flow velocity is tested by TEHN and compared to commercial flow velocity sensors. A signal processing module is designed to process the data locally without the need for a wired connection to a computer and acquisition module. Furthermore, a Power Management System (PMS) is designed to enhance the charging capability of the TENG. The charging voltage for a $4700\ \mu\text{F}$ capacitor can be increased from 2.4 to 24.6 V at the same time. A Lithium battery is charged

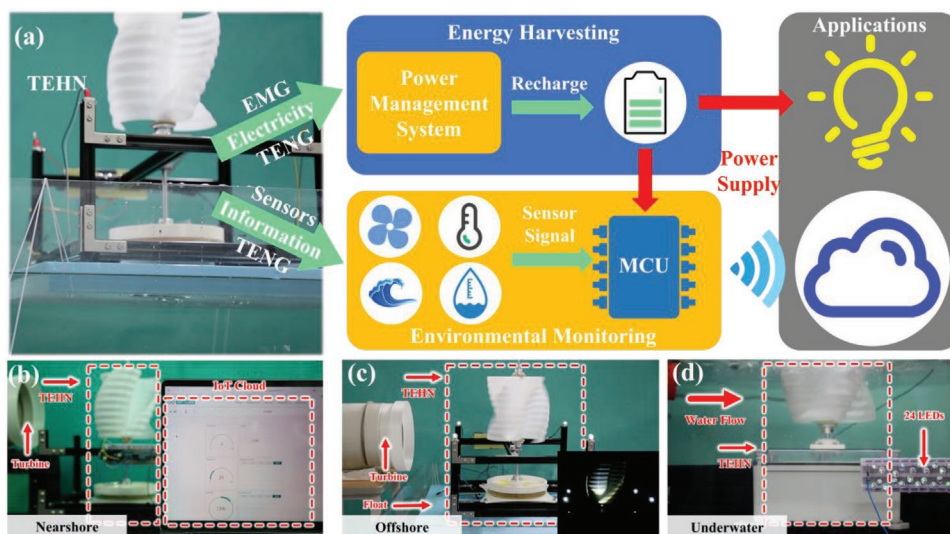


Figure 5. Application of the TEHN. a) The process flows from TEHN to applications. The photograph of TEHN work in nearshore (b), offshore (c), and underwater (d).

from 2.7 to 3.89 V through the TEHN, which can meet the power requirement of an MCU. Moreover, with an external timer, the MCU can automatically wake up and sleep. The continuous operation of the timer allows the sensor signals to be uploaded to the IoT periodically. Finally, the TEHN was successfully demonstrated in three scenarios: nearshore, offshore, and underwater. It is believed that the highly adaptive TEHN can provide a promising avenue for self-powered marine wireless monitoring.

4. Experimental Section

Fabrication of hybrid nanogenerator. The hybrid nanogenerator consisted of a TENG and an EMG, which both had a stator and rotor. The geometric model was designed through Solidworks software and produced by a 3D printer. As for the EMG, four NdFeB permanent disk magnets (50mm diameter and 5mm thickness) with the same magnetic pole laid in the same direction were inserted into the rotor. Four coils (2000 in turns, 0.1mm in diameter) were mounted on the stator. As for the TENG, six PVC films (150 μm in thickness) were fixed on the rotor. The electrodes of the TENG were fixed on the stator, and the copper film (50 μm thickness) had complementary sectors (12 sectors in total, with the same central angle, ≈29°).

Design of the TEHN supporting structure: In offshore and nearshore scenarios, aluminum profiles and fasteners were used to secure the TEHN. In underwater scenarios, a waterproof case and a dynamic seal (see Figure S4, Supporting Information) were applied.

Design of the waterproof treatment: The waterproof treatment was divided into two parts, static sealing and dynamic sealing. For the static sealing, a waterproof case to place TEHN, which was composed of PC and rubber and could provide a static seal. For the dynamic seal, the main part of the seal was the connection between the shaft and the waterproof box. The 3D printing technology to make a housing in which put O-rings and bearings to achieve the waterproof effect.

Electrical Measurement: An electrometer (6514, Keithley) with a LabVIEW program was used to measure the output performance of the TEHN. An AC servo motor controlled by an inverter (80ST-M02430, China) was used when testing different rotating speeds. Arduino MKR WIFI 1010 was selected to process the sensor signal and transmit the information through WIFI.

Supporting Information

Supporting Information is available from the Wiley Online Library or from the author.

Acknowledgements

Y.W., Z.Q., and C.Z. contributed equally to this work. The authors would like to thank the National Key R & D Project from the Minister of Science and Technology (2021YFA1201604), the National Natural Science Foundation of China (51879022, 52101382), and the Dalian Outstanding Young Scientific and Technological Talents Project (2021RJ11).

Conflict of Interest

The authors declare no conflict of interest.

Data Availability Statement

Research data are not shared.

Keywords

energy harvesting, hybrid nanogenerator, self-powered, triboelectric nanogenerator, wireless sensor nodes

Received: July 30, 2022

Revised: October 3, 2022

Published online:

- [1] M. Y. Durrani, R. Tariq, F. Aadil, M. Maqsood, Y. Nam, K. Muhammad, *Sensors* **2019**, *19*, 1145.
- [2] X. Deng, Y. Jiang, L. T. Yang, L. Yi, J. Chen, Y. Liu, X. Li, *IEEE Internet Things J.* **2020**, *7*, 9919.
- [3] T. Qiu, Z. Zhao, T. Zhang, C. Chen, C. L. Philip Chen, *IEEE Trans. Ind. Informatics* **2020**, *16*, 4297.
- [4] F. Adamo, F. Attivissimo, C. G. C. Carducci, L. Adamo, *IEEE Sens. J.* **2013**, *15*, 2514.
- [5] L. Yuan, X. Xiao, T. Ding, J. Zhong, X. Zhang, Y. Shen, B. Hu, Y. Huang, J. Zhou, Z. L. Wang, *Angew. Chem., Int. Ed.* **2012**, *51*, 4934.
- [6] M. Esteban, D. Leary, *Appl. Energy* **2012**, *90*, 128.
- [7] Y. Wang, X. Liu, T. Chen, H. Wang, C. Zhu, H. Yu, L. Song, X. Pan, J. Mi, C. Lee, M. Xu, *Nano Energy* **2021**, *90*, 106503.
- [8] Z. Zhou, X. Li, Y. Wu, H. Zhang, Z. Lin, K. Meng, Z. Lin, Q. He, C. Sun, J. Yang, Z. L. Wang, *Nano Energy* **2018**, *53*, 501.
- [9] B. Scrosati, *Chem. Rec.* **2005**, *5*, 286.
- [10] Y. Chen, X. Mu, T. Wang, W. Ren, Y. Yang, Z. L. Wang, C. Sun, A. Y. Gu, *Sci. Rep.* **2016**, *6*, 35180.
- [11] J. Wang, G. Zhao, M. Zhang, Z. Zhang, *Energy Sources, Part A Recover. Util. Environ. Eff.* **2018**, *40*, 1788.
- [12] Z. L. Wang, T. Jiang, L. Xu, *Nano Energy* **2017**, *39*, 9.
- [13] J. Wu, L. Qin, N. Chen, C. Qian, S. Zheng, *Energy* **2022**, *245*, 123318.
- [14] X. Shan, R. Song, B. Liu, T. Xie, *Ceram. Int.* **2015**, *41*, S763.
- [15] A. Mujtaba, U. Latif, E. Uddin, M. Y. Younis, M. Sajid, Z. Ali, A. Abdelkefi, *Appl. Energy* **2021**, *282*, 116173.
- [16] D. J. Olinger, Y. Wang, *J. Renew. Sustain. Energy* **2015**, *7*, 043114.
- [17] Y. Wang, X. Liu, Y. Wang, H. Wang, H. Wang, S. L. Zhang, T. Zhao, M. Xu, Z. L. Wang, *ACS Nano* **2021**, *15*, 15700.
- [18] H. Wu, Z. Wang, Y. Zi, *Adv. Energy Mater.* **2021**, *11*, 2100038.
- [19] L. Liu, X. Yang, L. Zhao, H. Hong, H. Cui, J. Duan, Q. Yang, Q. Tang, *ACS Nano* **2021**, *15*, 9412.
- [20] M. Xu, T. Zhao, C. Wang, S. L. Zhang, Z. Li, X. Pan, Z. L. Wang, *ACS Nano* **2019**, *13*, 1932.
- [21] H. Fu, X. Mei, D. Yurchenko, S. Zhou, S. Theodossiades, K. Nakano, E. M. Yeatman, *Joule* **2021**, *5*, 1074.
- [22] J. Zhu, M. Zhu, Q. Shi, F. Wen, L. Liu, B. Dong, A. Haroun, Y. Yang, P. Vachon, X. Guo, T. He, C. Lee, *EcoMat.* **2020**, *2*, e12058.
- [23] J. Luo, Z. L. Wang, *EcoMat.* **2020**, *2*, e12059.
- [24] T. Jiang, H. Pang, J. An, P. Lu, Y. Feng, X. Liang, W. Zhong, Z. L. Wang, *Adv. Energy Mater.* **2020**, *10*, 200064.
- [25] H. Wang, Z. Fan, T. Zhao, J. Dong, S. Wang, Y. Wang, X. Xiao, C. Liu, X. Pan, Y. Zhao, M. Xu, *Nano Energy* **2021**, *84*, 105920.
- [26] S. L. Zhang, M. Xu, C. Zhang, Y.-C. Wang, H. Zou, X. He, Z. Wang, Z. L. Wang, *Nano Energy* **2018**, *48*, 421.
- [27] J. An, Z. M. Wang, T. Jiang, X. Liang, Z. L. Wang, *Adv. Funct. Mater.* **2019**, *29*, 1904867.
- [28] X. Liang, T. Jiang, Y. Feng, P. Lu, J. An, Z. L. Wang, *Adv. Energy Mater.* **2020**, *10*, 2002123.
- [29] H. Wang, L. Xu, Y. Bai, Z. L. Wang, *Nat. Commun.* **2020**, *11*, 4203.
- [30] H. Hong, X. Yang, H. Cui, D. Zheng, H. Wen, R. Huang, L. Liu, J. Duan, Q. Tang, *Energy Environ. Sci.* **2022**, *15*, 621.
- [31] R. Xu, H. Wang, Z. Xi, W. Wang, M. Xu, *J. Mar. Sci. Eng.* **2022**, *10*, 566.

- [32] N. Khan, A. Kalair, N. Abas, A. Haider, *Renew. Sustain. Energy Rev.* **2017**, *72*, 590.
- [33] H. Mutsuda, Y. Tanaka, R. Patel, Y. Doi, Y. Moriyama, Y. Umino, *Appl. Ocean Res.* **2017**, *68*, 182.
- [34] V. Kumar, R. L. Shrivastava, S. P. Untawale, *Aquat. Procedia* **2015**, *4*, 473.
- [35] C. Ye, K. Dong, J. An, J. Yi, X. Peng, C. Ning, Z. L. Wang, *ACS Energy Lett.* **2021**, *6*, 1443.
- [36] P. Maharjan, T. Bhatta, H. Cho, X. Hui, C. Park, S. Yoon, M. Salauddin, M. T. Rahman, S. S. Rana, J. Y. Park, *Adv. Energy Mater.* **2020**, *10*, 2002782.
- [37] Z. Wen, H. Guo, Y. Zi, M.-H. Yeh, X. Wang, J. Deng, J. Wang, S. Li, C. Hu, L. Zhu, Z. L. Wang, *ACS Nano* **2016**, *10*, 6526.
- [38] B. Zhao, Z. Li, X. Liao, L. Qiao, Y. Li, S. Dong, Z. Zhang, B. Zhang, *Nano Energy* **2021**, *89*, 106381.
- [39] X. Zhong, Y. Yang, X. Wang, Z. L. Wang, *Nano Energy* **2015**, *13*, 771.
- [40] J. Wang, L. Pan, H. Guo, B. Zhang, R. Zhang, Z. Wu, C. Wu, L. Yang, R. Liao, Z. L. Wang, *Adv. Energy Mater.* **2019**, *9*, 1802892.
- [41] Y. Xi, H. Guo, Y. Zi, X. Li, J. Wang, J. Deng, S. Li, C. Hu, X. Cao, Z. L. Wang, *Adv. Energy Mater.* **2017**, *7*, 1602397.
- [42] P. Wang, L. Pan, J. Wang, M. Xu, G. Dai, H. Zou, K. Dong, Z. L. Wang, *ACS Nano* **2018**, *12*, 9433.
- [43] H. Guo, Z. Wen, Y. Zi, M. H. Yeh, J. Wang, L. Zhu, C. Hu, Z. L. Wang, *Adv. Energy Mater.* **2016**, *6*, 1501593.
- [44] J. Mu, H. He, J. Song, J. He, X. Hou, X. Han, C. Feng, J. Zou, J. Yu, X. Chou, *Energy Rep.* **2022**, *8*, 5272.
- [45] C. Wu, Q. Zhou, G. Wen, *Sens. Actuators, A* **2021**, *326*, 112723.
- [46] Q. Han, Z. Ding, W. Sun, X. Xu, F. Chu, *Sustain. Energy Technol. Assessments* **2020**, *39*, 100717.
- [47] S. Wang, Y. Xie, S. Niu, L. Lin, Z. L. Wang, *Adv. Mater.* **2014**, *26*, 2818.
- [48] S. Niu, Y. Liu, X. Chen, S. Wang, Y. S. Zhou, L. Lin, Y. Xie, Z. L. Wang, *Nano Energy* **2015**, *12*, 760.